



The effect of shape and size of ZnO nanoparticles on their antimicrobial and photocatalytic activities: a green approach

SAURABH SHARMA¹, KULDEEP KUMAR^{1,*} , NAVEEN THAKUR², S CHAUHAN³
and M S CHAUHAN³

¹Department of Chemistry, Career Point University, Hamirpur 176041, India

²Department of Physics, Career Point University, Hamirpur 176041, India

³Department of Chemistry, Himachal Pradesh University, Shimla 171005, India

*Author for correspondence (kuldeep.sharma.753@gmail.com)

MS received 21 December 2018; accepted 16 July 2019; published online 18 December 2019

Abstract. In this paper, ZnO nanoparticles (NPs) having potent photocatalytic and antimicrobial activities have been synthesized by using the aloe vera plant extract. The ZnO NPs have been synthesized using $(\text{Zn}(\text{CH}_3\text{COO})_2 \cdot 2\text{H}_2\text{O})$ (5, 10 and 50 mmol kg⁻¹), at temperature 70°C and pH 11.5. The synthesized NPs were examined using UV–Visible, X-ray diffraction, scanning electron microscopy, energy dispersive X-ray spectroscopy and transmission electron microscopy (TEM) characterization techniques. TEM analysis confirms the synthesis of ZnO NPs with hexagonal, spherical, cylindrical and cuboidal shapes decorated under different concentrations of precursor metal salt. UV–Visible studies revealed that ZnO NPs have a wide energy band gap varying from 3.36 to 3.43 eV. The synthesized ZnO NPs were examined for the photocatalytic degradation of methyl orange dye which resulted in up to 95% degradation. ZnO NPs are also inspected for the antibacterial activity against *Bacillus subtilis* (MTCC 441), *Staphylococcus aureus* (MTCC 737) and *Escherichia coli* (MTCC 739) pathogenic bacteria.

Keywords. Aloe vera; antimicrobial activity; green synthesis; methyl orange; zinc oxide nanoparticles.

1. Introduction

Zinc oxide (ZnO) nanoparticles (NPs) are well known for their wide range of applications. In the past few years, research on nanomaterials has been focused mainly on the synthesis and applications of ZnO NPs due to their excellent biocompatibility, low cost and low toxicity [1]. Further, the application efficiency of these NPs depends upon their physical and chemical aspects such as size, shape, surface state, crystal structure, attached moiety, dispensability, etc. [2,3]. Similarly, composites of NPs and doping with optical materials can be a tool for tailoring the band gap and other imperative properties [4]. Therefore, research in the field of methods of synthesis of NPs is oriented towards controlling their shape, size and composition as each parameter is a key aspect in defining the properties.

A number of methods, divided into three main categories such as physical, chemical and biological methods, have been exercised for the synthesis of ZnO NPs. Physical methods comprise the ball milling, laser ablation, chemical vapour deposition, etc. These methods require large energy, time and area, which make them inappropriate for the synthesis of NPs. In the chemical methods, there is use of harmful and toxic chemicals for the reduction and stabilization of NPs, which makes these methods unfriendly and unsustainable from the environmental point of view [5–8]. In the past, we can see

a consistent progress on the synthesis of ZnO NPs through the biological/green/plant extract method. The first research article on ZnO NP synthesis using latex of the *Calotropis procera* plant extract has been published in 2011 [9]. This method works on the reduction of the use of hazardous chemicals thereby leading to an energy efficient and low-temperature method for the synthesis of NPs.

Industrialization increases the evolution of various waste materials secreted in most of the water resources which results in the contamination of water and makes it hazardous. NPs are known for their valuable catalytic properties and are being used for the photocatalytic degradation of various waste water contaminations. Numerous metal NPs like gold, silver, platinum, palladium, etc. have been extensively used in the catalytic and electro-catalytic applications [6]. Although these metals showed significant achievements in catalysis, they are not economical, and so this demands the need for the synthesis of economical metal NPs like ZnO [10]. In addition to catalysis, ZnO NPs are also employed in the medical field as NPs are proficient antimicrobial agents. Currently, several pathogenic bacteria have developed that cause an adverse impact on health. NPs have been proved to be an effective tool to inhibit these pathogenic bacteria which show resistance to most of the commercially available antibiotics [11].

Therefore, in the present work, we have attempted to implement the green method for the synthesis of ZnO NPs using the

aloe vera leaf extract. The synthesized ZnO NPs have been successfully employed as photocatalysts in dye degradation and antimicrobial agents against the three different pathogenic bacteria.

2. Materials and methods

2.1 Materials

Deionized distilled water with a conductivity of $2\text{--}3 \times 10^{-6} \text{ S cm}^{-1}$ and a pH of 6.8–7.0 (at 298.15 K) was used for all experiments. Zinc acetate di-hydrate ($\text{Zn}(\text{CH}_3\text{COO})_2 \cdot 2\text{H}_2\text{O}$), potassium hydroxide (KOH) and methyl orange (MO) dye were obtained from Merck Pvt. Ltd. and were used as such without further purification. Microbes *Bacillus subtilis* (MTCC 441), *Staphylococcus aureus* (MTCC 737) and *Escherichia coli* (MTCC 739) were obtained from the CSIR-IMTECH, Chandigarh, in the form of freeze dried ampoule. Aloe vera plant leaves were collected from the nearby area of Career Point University Hamirpur (HP).

2.2 Methods

2.2a Preparation of the aloe vera leaf extract: Fresh leaf aloe vera plants were collected, weighed (25 g) and washed with tap water and then with distilled water to remove the impurities. The washed leaves were crushed and boiled for about 15 min in 100 ml distilled water. The boiled extract was cooled and filtered through Whatman filter paper. The filtered plant extract solution was used for the synthesis of ZnO NPs. The plant extract was stored in a refrigerator for further use [12].

2.2b Synthesis of ZnO NPs: Aqueous solutions of zinc acetate di-hydrate (5, 10 and 50 mmol kg^{-1}) were prepared using distilled water. The above-prepared aloe vera plant extract was added dropwise to these solutions ($\sim 5 \text{ ml min}^{-1}$) in a round bottom flask under constant stirring and heating at 70°C. About 15 min after the addition, freshly prepared 0.2 mol kg^{-1} KOH solution was added dropwise to the reaction mixture to maintain the pH of 11.5. The formation of ZnO NPs was confirmed by the appearance of yellowish white colour precipitates in the solution mixture. After constant stirring and heating for 4 h, the ZnO NPs were collected and washed 3–4 times with distilled water and then with ethanol. The NPs were dried in a hot air oven at 55–60°C before further use.

2.2c Characterization of NPs: The synthesis of ZnO NPs has been confirmed from the UV–visible spectra of the compounds. X-ray powder diffraction (XRD) has been used for determining the crystallinity, phase and phase purity of the NPs. A field emission-scanning electron microscope (FE-SEM) was used for the morphological studies with the SEM-energy dispersive X-ray spectroscopy (EDS) for elemental detection analysis. Transmission electron microscopy (TEM) was used for the shape and size determination of the ZnO NPs.

2.2d Antimicrobial activity: The antimicrobial activity of the synthesized ZnO NPs was determined using well diffusion assay (NCCLS) [13] against the three different pathogens namely, *B. subtilis* (MTCC 441), *S. aureus* (MTCC 737) and *E. coli* (MTCC 739). The isolated colonies were collected from an agar plate and transferred into a test tube which contains autoclaved 0.85% saline solution. The turbidity of inoculum (test tube solution) was compared with 0.5 McFarland standards so that inoculum contains $1\text{--}2 \times 10^8 \text{ CFU ml}^{-1}$. Mueller Hinton agar (MHA) plates were prepared and a sterilized cotton swab was dipped into inoculum and swab streaked over the entire surface of MHA plates for each inoculum. The wells were made on the plates and different concentrations of the synthesized ZnO NP solution (w/v) prepared in methanol were loaded into the wells by taking methanol as the negative control and ciprofloxacin ($100 \mu\text{g ml}^{-1} \text{ w/v}$) as the positive control. The plates were incubated at 37°C for 24 h. After incubation, the zones of inhibitions were measured and reported.

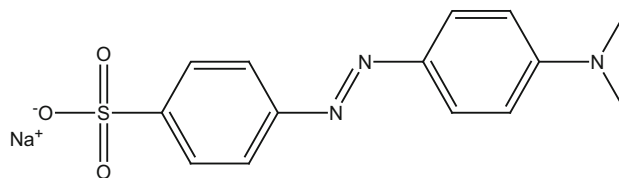


Figure 1. Chemical structure of MO.

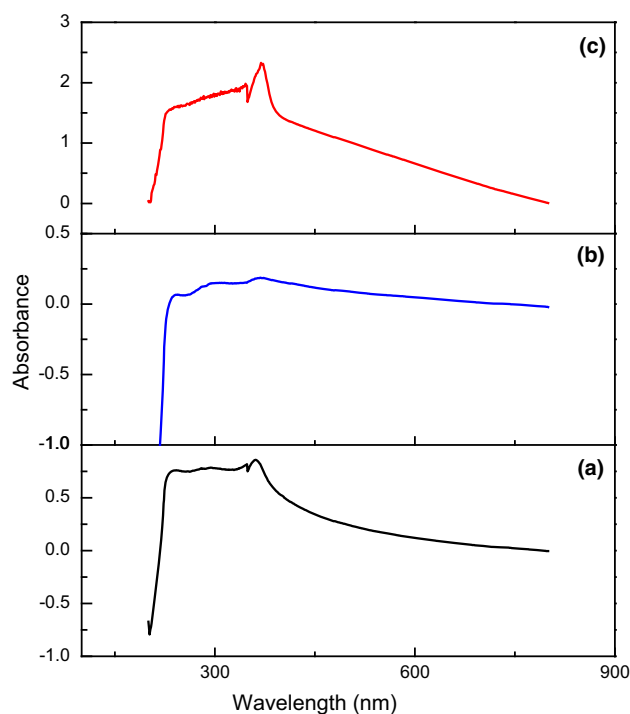


Figure 2. UV–visible spectra of ZnO NPs at different concentrations of $\text{Zn}(\text{CH}_3\text{COO})_2 \cdot 2\text{H}_2\text{O}$: (a) 5, (b) 10 and (c) 50 mmol kg^{-1} .

Further, the minimum inhibitory concentration (MIC) and minimum bactericidal concentration (MBC) of the synthesized ZnO NPs have been measured by using the broth micro dilution method (CLSI) [13]. In this test, double strength Mueller-Hinton broth (MHB) and $2\times$ (double concentration) solution of ZnO NPs were prepared. Each well of the 96-well micro-titer plate was loaded with $100\ \mu\text{l}$ of MHB. Then, $100\ \mu\text{l}$ of ZnO NPs ($2\times$) were added into the first well and

Table 1. λ_{max} and energy band gap (E_g) values of ZnO NPs at different concentrations of $\text{Zn}(\text{CH}_3\text{COO})_2\cdot 2\text{H}_2\text{O}$.

m^a (mmol kg^{-1})	λ_{max} (nm)	E_g (eV)
5	361	3.435
10	368	3.370
50	369	3.360

^a m is the molality of $\text{Zn}(\text{CH}_3\text{COO})_2\cdot 2\text{H}_2\text{O}$ in water.

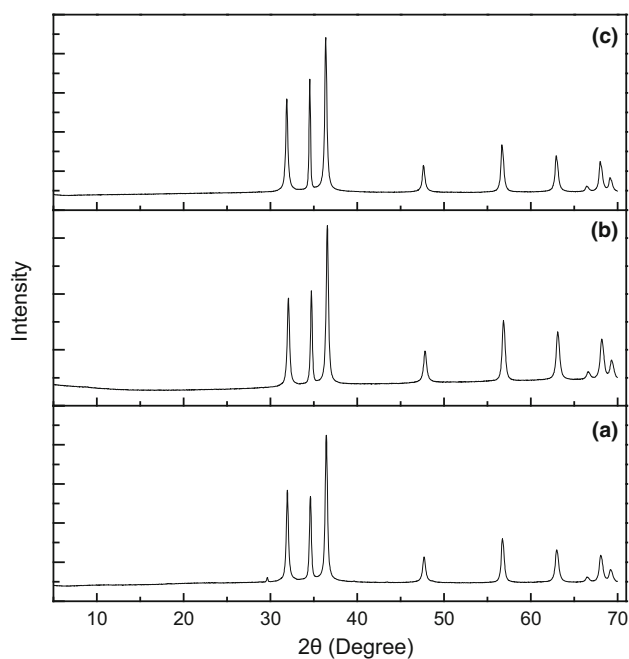


Figure 3. XRD patterns of ZnO NPs at different concentrations of $\text{Zn}(\text{CH}_3\text{COO})_2\cdot 2\text{H}_2\text{O}$: (a) 5, (b) 10 and (c) 50 mmol kg^{-1} .

serial dilutions were made up to the ninth well. After this, $30\ \mu\text{l}$ inoculums were added to each well. The 10th well was taken as the growth control well (containing MHB and inoculum only), 11th well as the negative control (containing MHB and inoculum with methanol) and 12th well was taken as the positive control (containing MHB and inoculum with ciprofloxacin). Micro-titer plates were incubated at 37°C for 24 h. The lowest concentration that shows visual inhibition of growth was considered as the MIC of the ZnO NPs for the respective organism. For the MBC measurements, $10\ \mu\text{l}$ of suspension from each well of the micro-titer plate was inoculated on a nutrient agar plate at 37°C for 24 h. The concentration of ZnO NPs, which show the absence of colonies on the agar plates, was taken as the MBC for the respective NPs.

2.2e Photocatalytic degradation of dye: To investigate the photocatalytic activity of the synthesized ZnO NPs, $100\ \text{ml}$ of $10\ \text{ppm}$ MO (figure 1) solution was treated with 25, 50 and $100\ \text{mg}$ of ZnO NP catalytic loads distinctly for 160 min in the presence of UV light. The decomposition of MO was examined by the rate of dye degradation estimated by evaluating the change in absorbance in the UV–Visible spectrophotometer Cary 100 Bio at $\lambda = 465\ \text{nm}$ [14].

3. Results and discussion

3.1 UV–visible spectroscopic analysis

The optical properties of the synthesized ZnO NPs have been investigated by carrying out UV–visible spectroscopy measurements in an interval of $200\text{--}800\ \text{nm}$. The clear suspension solutions of NPs in methanol were prepared by using a sonicator. The UV–visible spectra of the synthesized NPs at different concentrations of $\text{Zn}(\text{CH}_3\text{COO})_2\cdot 2\text{H}_2\text{O}$ (5, 10 and $50\ \text{mmol kg}^{-1}$) (figure 2) show a hump near $370\ \text{nm}$, which is the characteristic peak of the ZnO NPs [15]. The optical energy band gap (E_g) given in table 1 was calculated as:

$$E_g = \frac{hc}{\lambda} \quad (1)$$

where h is Planck's constant = $6.626 \times 10^{-34}\ \text{J s}$, C is the velocity of light = $3 \times 10^8\ \text{m s}^{-1}$ and λ corresponds

Table 2. Crystallite size (D), inter-planar spacing (d), lattice parameters ($a = b$ and c) and volume (V) calculated from XRD measurements at different concentrations of $\text{Zn}(\text{CH}_3\text{COO})_2\cdot 2\text{H}_2\text{O}$.

m^a (mmol kg^{-1})	D (nm)	d (nm)	$a = b$ (nm)	c (nm)	V (nm^3)
5	30.145	0.246	0.323	0.517	4.677
10	30.155	0.246	0.322	0.516	4.626
50	30.349	0.247	0.324	0.519	4.711

^a m is the molality of zinc acetate di-hydrate in water.

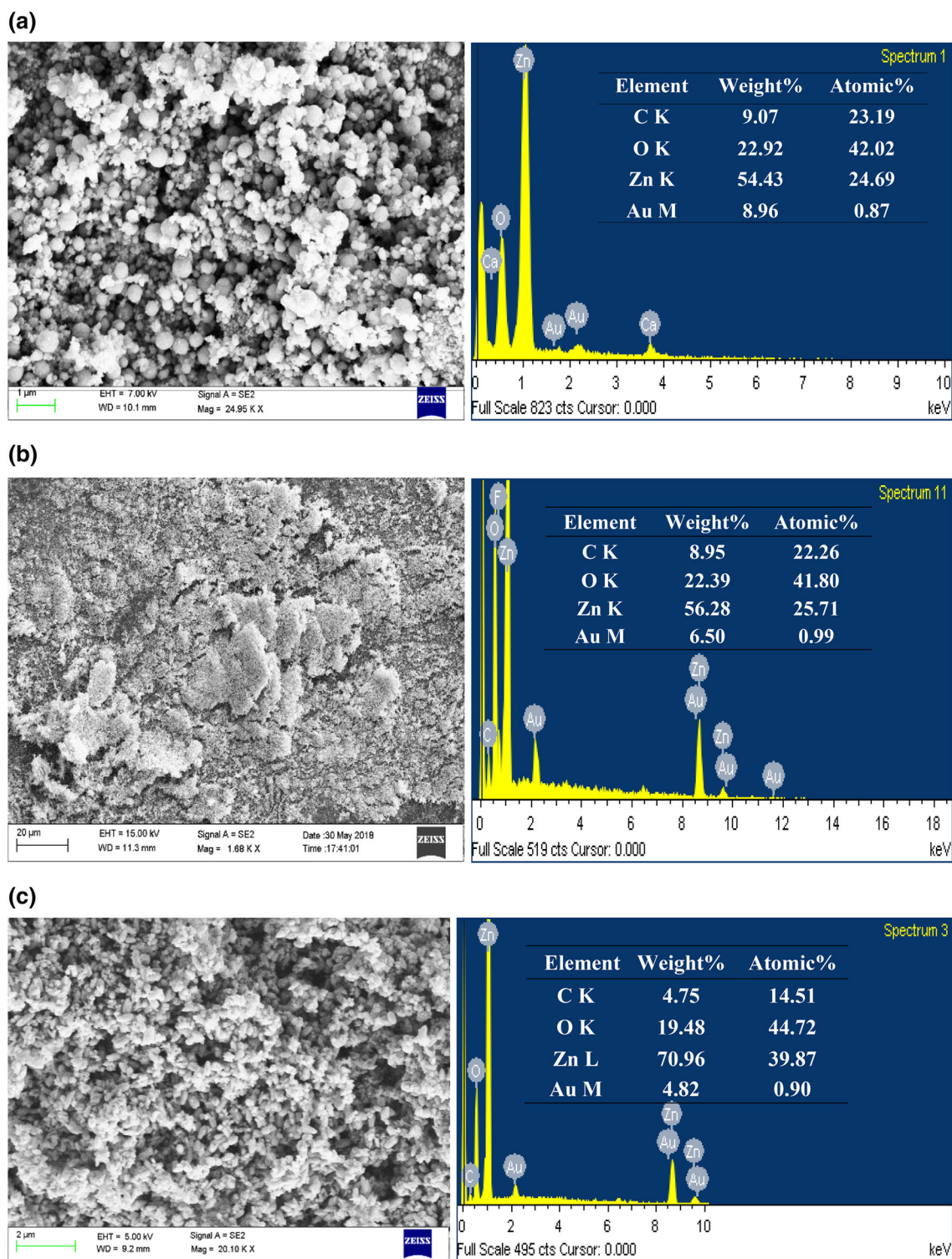


Figure 4. SEM/EDS spectra of ZnO NPs at different concentrations of $\text{Zn}(\text{CH}_3\text{COO})_2 \cdot 2\text{H}_2\text{O}$: (a) 5, (b) 10 and (c) 50 mmol kg^{-1} .

to the wavelength of the peak with the maximum intensity [16].

The band gap values are found to be approximately equal to 3.4 eV, which is in accordance with the literature. Similar

band gap values are reported by Suresh *et al* (3.33 eV) [17] and Hancock *et al* (3.39 eV) [18]. The change in the value of E_g with concentration of $\text{Zn}(\text{CH}_3\text{COO})_2 \cdot 2\text{H}_2\text{O}$ can be attributed to the change in the shape/size of the ZnO NPs. Further,

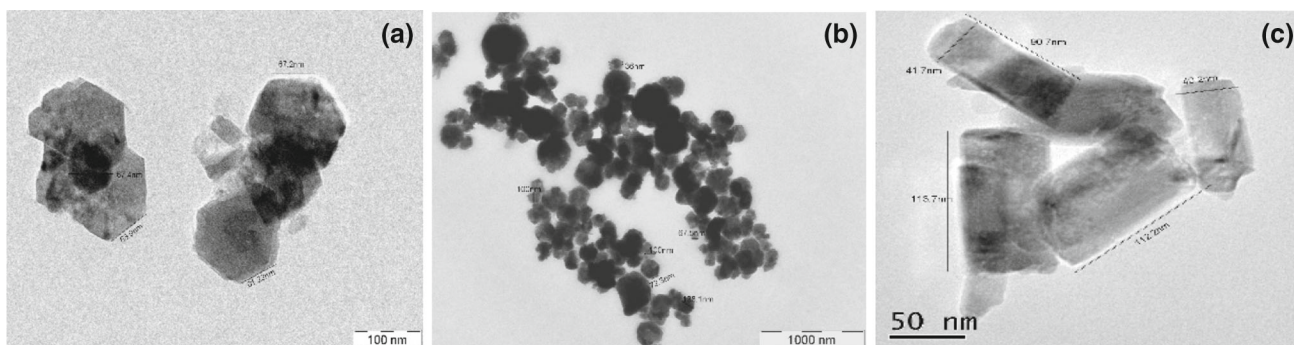


Figure 5. TEM images of ZnO NPs at different concentrations of $Zn(CH_3COO)_2 \cdot 2H_2O$: (a) 5, (b) 10 and (c) 50 $mmol\ kg^{-1}$.

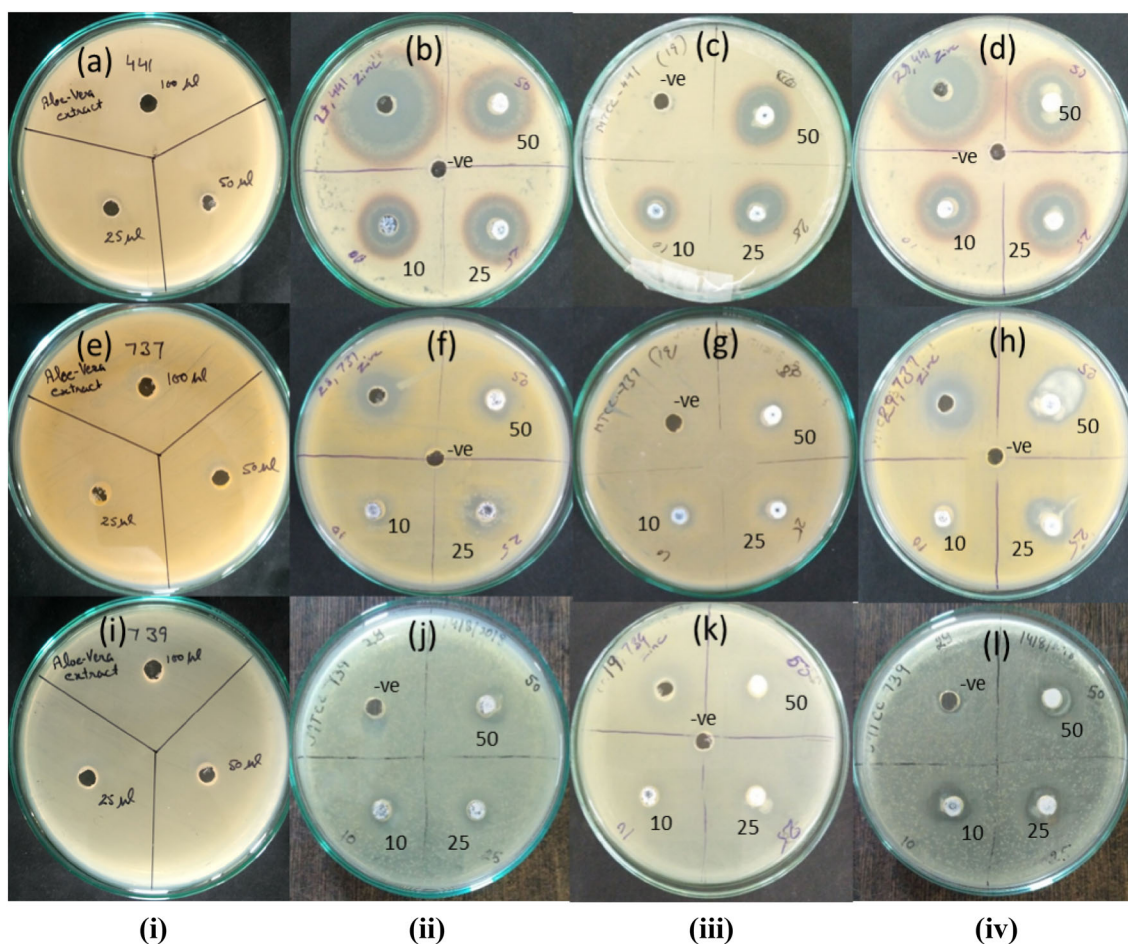


Figure 6. (i) Antibacterial activity of the aloe vera leaf extract and ZnO NPs at different concentrations of $Zn(CH_3COO)_2 \cdot 2H_2O$: (ii) 5, (iii) 10 and (iv) 50 $mmol\ kg^{-1}$ against (a–d) *B. subtilis*, (e–h) *S. aureus* and (i–l) *E. coli*, respectively.

a decrease in E_g values is the result of the increase in the particle size [19].

3.2 XRD analysis

XRD analysis has been carried out to confirm the crystalline nature, phase purity and formation of the hexagonal wurtzite

crystal system of the synthesized ZnO NPs. XRD patterns (figure 3) show peaks at angle $2\theta \approx 31, 34, 36, 47, 56, 63, 66, 68$ and 69° , which correspond to (100), (002), (101), (102), (110), (103), (200), (112) and (201) crystal planes of ZnO NPs. Similar planes are reported by Hameed *et al* [20] for the ZnO NPs. In the spectra, no extra peaks have been seen except the peaks for the ZnO NPs, which confirm the phase

purity of all the synthesized ZnO NPs. An XRD technique also determines the structural arrangement of the particles and shape and size of the unit cell of the compound. Clear and sharp peaks at the definite positions explain the hexagonal crystal nature with the wurtzite structure of all the synthesized ZnO NPs. The crystallite size (D) of the NPs is determined by taking the full width at half maximum (FWHM) of the most intense peak using the Debye–Scherrer equation (2) [20]. Inter-planar spacing (d), lattice parameters ($a = b$ and c) for the hexagonal wurtzite structure and volume of the hexagonal system unit cell (V) have been calculated by using the Bragg's equations (3–5), respectively [21–23]. All these parameters are summarized in table 2.

$$D = \frac{0.94\lambda}{\beta \cos \theta} \quad (2)$$

$$n\lambda = 2d \sin \theta \quad (3)$$

$$\frac{1}{d_{hkl}^2} = \frac{4}{3} \left(\frac{h^2 + hk + k^2}{a^2} \right) + \frac{l^2}{c^2} \quad (4)$$

$$V = \frac{\sqrt{3}}{2} a^2 c \quad (5)$$

where $\lambda = 1.5406 \text{ \AA}$, $\beta = \text{FWHM}$, $\theta = \text{Bragg's angle}$, $(hkl) = \text{Miller indices}$, $d_{hkl} = \text{inter-planar spacing}$, $V = \text{volume of the unit cell}$ and $a, c = \text{lattice parameters for the ZnO NP hexagonal system}$.

The data reported in table 2 are closely related to the literature with a slight variation due to the different shapes and sizes of ZnO NPs [24]. The crystallite size (D) of ZnO NPs slightly increases on increasing the $\text{Zn}(\text{CH}_3\text{COO})_2 \cdot 2\text{H}_2\text{O}$

Table 3. The zones of inhibition of the prepared aloe vera leaf extract and synthesized ZnO NPs at different concentrations of $\text{Zn}(\text{CH}_3\text{COO})_2 \cdot 2\text{H}_2\text{O}$.

Bacteria	m ^a (mmol kg ⁻¹)	NPs dosage (mg ml ⁻¹)	Zone of inhibition (mm)	
<i>B. subtilis</i>	5	10	13.50 ± 0.5 ^b	
		25	14.25 ± 0.25	
		50	15.23 ± 0.07	
	10	10	14.26 ± 0.15	
		25	15 ± 0.58	
		50	15.93 ± 0.54	
	50	10	15.80 ± 0.8	
		25	16.85 ± 0.85	
		50	18.53 ± 0.77	
	<i>S. aureus</i>	Aloe vera leaf extract	25/50/100 µl per well	No zone of inhibition
		Ciprofloxacin	Ciprofloxacin 0.1 mg ml ⁻¹	35 ± 1
		5	10	8.90 ± 0.6
25			10.10 ± 0.4	
50			10.75 ± 0.25	
10		10	8.90 ± 0.58	
		25	9.10 ± 0.61	
		50	9.75 ± 0.43	
50		10	9.70 ± 0.1	
		25	10.50 ± 0.5	
		50	11.40 ± 0.6	
<i>E. coli</i>		Aloe vera leaf extract	25/50/100 µl per well	No zone of inhibition
	Ciprofloxacin	Ciprofloxacin 0.1 mg ml ⁻¹	30 ± 1.2	
	5	10	9.50 ± 0.5	
		25	10.65 ± 0.65	
		50	11.30 ± 0	
	10	10	8.89 ± 0.11	
		25	9.33 ± 0.33	
		50	10.56 ± 0.43	
	50	10	9.25 ± 0.25	
		25	10.25 ± 0.25	
		50	11.65 ± 0.35	
	Aloe vera leaf extract	25/50/100 µl per well	No zone of inhibition	
Ciprofloxacin	Ciprofloxacin 0.1 mg ml ⁻¹	33 ± 0.7		

^am is the molality of zinc acetate di-hydrate in water.

^bStandard error in measurement of zone of inhibition.

concentration, however, the inter-planar spacing (d) values are unchanged.

3.3 SEM/EDS spectral analysis

The SEM images provide the morphological representations of the synthesized ZnO NPs as illustrated in figure 4. These images inferred that the ZnO NPs synthesized at 50 mmol kg⁻¹ concentration of zinc acetate dihydrate are cylindrical in shape, whereas at both 5 and 10 mmol kg⁻¹ concentrations the NPs look like spherical in shape.

The peaks in the EDS spectra illustrated in figure 4 confirm the presence of Zn and O in all the synthesized ZnO NPs. However, peaks corresponding to Au may be due to gold coating used in SEM/EDS micrograph analysis. The peak corresponding to elemental carbon may be attributed to the carbon tape or organic molecules from the aloe vera leaf extract which are involved in the stabilization of ZnO NPs. Samat and Nor [25] also reported spherical-shaped ZnO NPs with a size of 50–200 nm by using the sol–gel method of green synthesis. On the other hand, Elangovan *et al* [26] have used the chemical synthesis method and reported the spherical- to rod-shaped ZnO NPs.

3.4 TEM analysis

Figure 5 represents the TEM images of ZnO NPs synthesized at different concentrations of Zn(CH₃COO)₂·2H₂O. From analysis of TEM images, it can be concluded that the shape and size of ZnO NPs vary with the concentration of Zn(CH₃COO)₂·2H₂O. At 5 mmol kg⁻¹ the shape of NPs is hexagonal with an average size of ~63 nm. A little variation

in the shape and size of the particles has been observed at 10 mmol kg⁻¹ and particles were spherical and hexagonal in shape. However, the average sizes of the particles are ~65 and 60–180 nm for hexagonal- and spherical-shaped particles, respectively. Finally, at 50 mmol kg⁻¹ cuboidal/rod-shaped particles with an average size of 40–45 nm are obtained. Thus, there is a transformation in the shape of NPs on increasing the concentration of Zn(CH₃COO)₂·2H₂O. Wang *et al* [27] have also coined similar results with distorted spherical-shaped particles and explained that the shape of ZnO NPs changed from rods to globular with a decrease in the particle size, as the concentration of ZnCl₂ solution increased.

3.5 Antimicrobial activity

The agar well diffusion method [13] has been applied to examine the antimicrobial activity of the synthesized NPs. The activities of the ZnO NPs for the *B. subtilis* (MTCC 441), *S. aureus* (MTCC 737) and *E. coli* (MTCC 739) have been investigated on the MHA. The zones of inhibition of the prepared aloe vera leaf extract and synthesized ZnO NPs (figure 6) have been measured for each bacteria and are summarized in table 3. It has been noticed that the prepared aloe vera leaf extract has shown no zone of inhibition for all the studied bacteria (figure 6), which may be attributed to the low concentration of the leaf extract. However, from table 3, it can be seen that the largest zone of inhibition for all the synthesized ZnO NPs has been generally obtained for *B. subtilis*, which is followed by *E. coli* and *S. aureus*, respectively.

The biological activity with respect to the microbes has been evaluated for 10, 25 and 50 mg ml⁻¹ ZnO NPs in methanol as the solvent. 30 μl of solution of ZnO NPs

Table 4. MIC and MBC values of ZnO NPs and ciprofloxacin for different bacteria under study.

Bacteria	m ^a (mmol kg ⁻¹)	MIC (μg ml ⁻¹)	MBC (μg ml ⁻¹)
<i>B. subtilis</i>	5	391 (895.18) ^b	12500
	10	391	6250
	50	195	12500
	Ciprofloxacin	< 1	< 0.5
<i>S. aureus</i>	5	781 (732.42) ^b (1000) ^c	6250
	10	391	6250
	50	391	12500
	Ciprofloxacin	16.65	1
<i>E. coli</i>	5	1562 (1708.98) ^b (3400) ^c	12500
	10	1562	12500
	50	1562	12500
	Ciprofloxacin	< 1	0.5

^am is the molality of zinc acetate dihydrate in water.

^bRef [29].

^cRef [7].

was loaded into the wells by taking the methanol as the negative control and ciprofloxacin ($100 \mu\text{g ml}^{-1}$ w/v) as the positive control. On comparison, the cuboidal-shaped ZnO NPs are found to be relatively more effective as compared to other NPs. The values of MIC and MBC have been calculated by using the 96th well micro-titer plate and are tabulated in table 4. The MIC and MBC value ranges between 195 and $3125 \mu\text{g ml}^{-1}$ and 6250 and $12500 \mu\text{g ml}^{-1}$, respectively. Lingaraju *et al* [23] and Prashanth *et al* [21] have reported similar results for the antibacterial activity of ZnO NPs synthesized using *Ruta graveolens* and *Punica granatum/Tamarindus indica*, respectively. Kronvall has reported the results, which are in favour of our findings on the zone of inhibition, MIC and MBC values for the ciprofloxacin [28]. Further, if we compare MIC values of ZnO

NPs synthesized by using chemical methods, as mentioned in the parenthesis of table 4 [7,29], we found that these values are greater than the values calculated in the present study. These observations clearly show that the plant-mediated ZnO NPs are more efficient antibacterial agents.

3.6 Photocatalytic degradation of MO dye

The synthesized NPs have been investigated as photocatalysts for the degradation of MO (10 ppm) in the presence of UV light. MO shows absorbance in UV-visible light at 465 nm. In the presence of catalyst and UV light, the degradation of dye has been studied as a function of decrease in the intensity of the absorption peak of MO at 465 nm with the passage of time (figure 7).

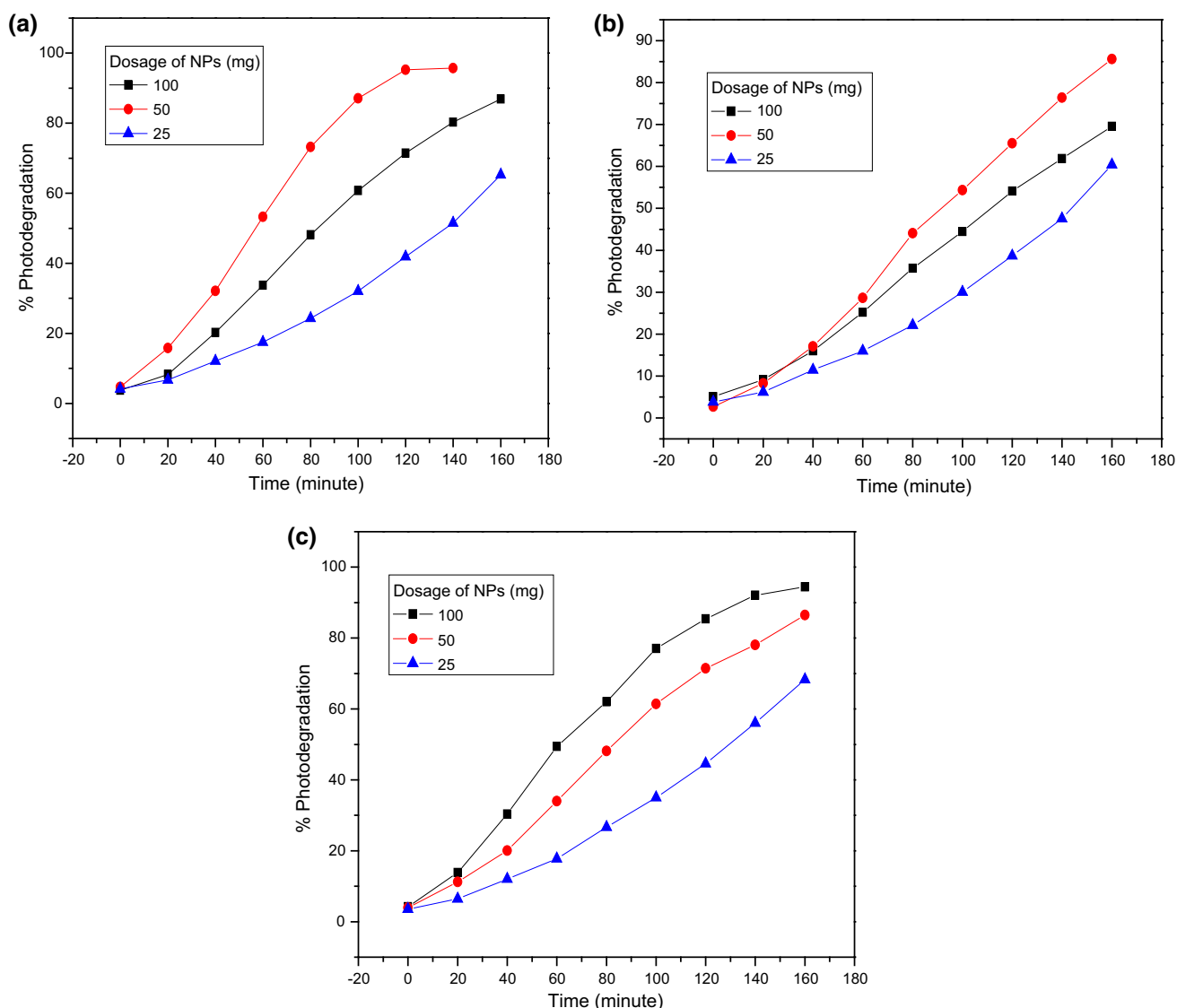


Figure 7. Percentage photodegradation of 10 ppm MO dye with the passage of time in the presence of ZnO NPs at different concentrations of $\text{Zn}(\text{CH}_3\text{COO})_2 \cdot 2\text{H}_2\text{O}$: (a) 5, (b) 10 and (c) 50 mmol kg^{-1} .

Table 5. Percentage of photocatalytic degradation of 100 ml of 10 ppm MO dye solution at different dosages of ZnO NPs.

m^a (mmol kg ⁻¹)	NPs dosage (mg)	Time (min)	Percentage of photocatalytic degradation of MO dye (%)
5	25	160	65.3
	50	140	95.7
	100	160	86.9
10	25	160	60.4
	50	160	85.6
	100	160	69.6
50	25	160	68.3
	50	160	86.5
	100	160	94.4

^a m is the molality of zinc acetate di-hydrate in water.

The UV light plays an efficient role in the degradation of the dye and the degradation can easily be examined by the decolourisation of the dye solution in the presence of NPs. On increasing the UV irradiation time, there is efficient photocatalytic degradation of the dye solution as examined with the help of a UV-Visible spectrophotometer. The percentage degradation of dye was calculated from the following relationship

$$\% \text{Degradation} = \frac{A_0 - A_t}{A_0} \times 100 \quad (6)$$

where A_0 is the absorbance of pure dye solution and A_t is the absorbance of the reaction mixture at time t .

The results of degradation of dye MO (table 5) revealed that the catalytic efficiency of hexagonal- and spherical-shaped ZnO NPs (i.e., for $[\text{Zn}(\text{CH}_3\text{COO})_2 \cdot 2\text{H}_2\text{O}] = 5$ and 10 mmol kg^{-1}) follows the order of catalytic load as $50 > 100 > 25 \text{ mg}$ for 100 ml of 10 ppm MO solution, whereas in the case of cuboidal-shaped ZnO NPs (i.e., for $[\text{Zn}(\text{CH}_3\text{COO})_2 \cdot 2\text{H}_2\text{O}] = 50 \text{ mmol kg}^{-1}$) the order of catalytic load is $100 > 50 > 25 \text{ mg}$. This order can be attributed to the morphology of the spherical/hexagonal-shaped ZnO NPs that provide the large interstitial space to accommodate the dye molecules and undergo degradation much more efficiently at 50 mg load. Moreover, the photocatalytic degradation efficiency depends on the active surface area of the photo-catalyst. It has been reported that the photocatalytic degradation efficiency increases as the amount of the photo-catalyst increases but after a certain value there is a decrease in degradation [30]. This outcome can be explained as, after a peak value, an increment in the catalytic amount can lead to an increase in the turbidity and scattering effects, causing less UV light penetration. Also at high concentration, the photo-catalyst NPs have a tendency to aggregate, which reduces the number of active sites [31]. Khataee *et al* [32] have reported similar results in which degradation increases with a catalyst dosage up to 1 g l^{-1} and then a decrease in the degradation

efficiency has been observed with a further increase in the catalyst dosage from 1 to 2 g l^{-1} .

4. Conclusions

The present study provides a cost effective and eco-friendly method for the synthesis of ZnO NPs as potent photo-catalysts and antimicrobial agents. The TEM images revealed that the shapes of the synthesized NPs varied with the concentration of the originator $\text{Zn}(\text{CH}_3\text{COO})_2 \cdot 2\text{H}_2\text{O}$. However, the size of NPs ranges from 40 to 180 nm. The synthesized ZnO NPs have been assessed for their antibacterial activities against three bacteria, *B. subtilis*, *E. coli* and *S. aureus*. The largest zone of inhibition has been attained generally for *B. subtilis*, which is followed by *E. coli* and *S. aureus*, respectively. Further, the MIC and MBC values lie between 195 and $3125 \mu\text{g ml}^{-1}$ and 6250 and $12500 \mu\text{g ml}^{-1}$, respectively. The cuboidal-shaped NPs were found to be more protuberant in antibacterial activities as compared to spherical- and hexagonal-shaped NPs. The synthesized ZnO NPs show tremendous catalytic activities for the degradation of dye MO in the presence of UV light. Up to 95% degradation of the dye MO in the time interval of 140–160 min has been observed in the presence of NPs as catalysts. The shape of the NPs played a vital role in photo-catalysis. For the spherical- and hexagonal-shaped particles, 50 mg catalytic load for 100 ml of 10 ppm MO dye solution is more effective than the 100 and 25 mg catalytic load. However, for cuboidal-shaped NPs, on increasing the catalytic load from 25 to 100 mg, the degradation efficiency goes on increasing.

References

- [1] Jiang J, Pi J and Cai J 2018 *Bioinorg. Chem. Appl.* **18** 1
- [2] An L J, Wang J, Zhang T F, Yang H L and Sun Z H 2012 *Adv. Mater. Res.* **380** 338

- [3] Bhooshan K V and Paik P 2017 *Adv. Mater. Lett.* **8** 493
- [4] Wahab R, Ansari S G, Kim Y-S, Seo H-K and Shin H-S 2007 *Appl. Surf. Sci.* **253** 7622
- [5] Sabir S, Arshad M and Chaudhari S K 2014 *Sci. World J.* **14** 1
- [6] Udayabhanu, Nagaraju G, Nagabhushana H, Basavaraj R B, Raghu G K, Suresh D *et al* 2016 *Cryst. Growth Des.* **16** 6828
- [7] Sirelkhatim A, Mahmud S, Seeni A, Kaus N H M, Ann L C, Bakhori S K M *et al* 2015 *Nano-Micro Lett.* **7** 219
- [8] Naveed A H U, Nadhman A, Ullah I, Mustafa G, Yasinzaï M and Khan I 2017 *J. Nanomater.* **2017** 1
- [9] Singh R P, Shukla V K, Yadav R S, Sharma P K, Singh P K and Pandey A C 2011 *Adv. Mater. Lett.* **2** 313
- [10] Surendra T V, Roopan S M, Al-Dhabi N A, Arasu M V, Sarkar G and Suthindhiran K 2016 *Nanoscale Res. Lett.* **11** 1
- [11] Anbukkarasi V, Srinivasan R and Elangovan N 2015 *Int. J. Pharm. Sci. Rev. Res.* **33** 110
- [12] Supraja N, Prasad T N V K V, Krishna T G and David E 2016 *Appl. Nanosci.* **6** 581
- [13] Balouiri M, Sadiki M and Ibsouda S K 2016 *J. Pharm. Anal.* **6** 71
- [14] Sharma P, Kumar R, Chauhan S, Singh D and Chauhan M S 2014 *J. Nanosci. Nanotechnol.* **4** 6153
- [15] Singh V, Mohan L, Baranwal K, Asthana S and Sundaram S 2018 *Appl. Nanosci.* **8** 1149
- [16] Choudhary M K, Kataria J and Sharma S 2018 *Appl. Nano Mater.* **1** 1870
- [17] Suresh D, Nethravathi P C, Udayabhanu, Rajanaika H, Nagabhushana H and Sharma S C 2015 *Mater. Sci. Semicond. Process.* **31** 446
- [18] Hancock J M, Rankin W M, Hammad T M, Salem J S, Chesnel K and Harrison R G 2015 *J. Nanosci. Nanotechnol.* **15** 3809
- [19] Akbarian M, Mahjoub S, Elahi S M, Zabihi E and Tashakkorian H 2018 *New J. Chem.* **42** 5822
- [20] Hameed A S H, Karthikeyan C, Ahamed A P, Thajuddin N, Alharbi N S, Alharbi S A *et al* 2016 *Sci. Rep.* **6** 1
- [21] Prashanth G K, Prashanth P A, Utpal B, Manoj G, Nagabhushana B M, Ananda S *et al* 2015 *Int. J. Mod. Sci.* **1** 67
- [22] Khorsand Zak A, Abd. Majid W H, Abrishami M E and Yousefi R 2011 *Solid State Sci.* **13** 251
- [23] Lingaraju K, Raja Naika H, Manjunath K, Basavaraj R B, Nagabhushana H, Nagaraju G *et al* 2016 *Appl. Nanosci.* **6** 703
- [24] Lakshmeesha T R, Sateesh M K, Prasad B D, Sharma S C, Kavyashree D, Chandrasekhar M *et al* 2014 *Cryst. Growth Des.* **14** 4068
- [25] Samat A N and Nor M R 2013 *Ceram. Int.* **39** 545
- [26] Elangovan S V, Chandramohan V, Sivakumar N and Senthil T S 2016 *Desalin. Water Treat.* **57** 9671
- [27] Wang Z, Li H, Tang F, Ma J and Zhou X 2018 *Nanoscale Res. Lett.* **13** 1
- [28] Kronvall G 2000 *Clin. Microbiol. Infect.* **6** 483
- [29] Shahid S, Khan S A, Ahmad W, Fatima U and Knawal S 2017 *Indian J. Pharm. Sci.* **80** 173
- [30] Hassan S S M, Azab W I M E, Ali H R and Mansour M S M 2015 *Adv. Nat. Sci.: Nanosci. Nanotechnol.* **6** 1
- [31] Modirshahla N, Hassani A, Behnajady M A and Rahbarfam R 2011 *Desalination* **271** 187
- [32] Khataee A, Soltani R D C, Hanifehpour Y, Safarpour M, Gholipour Ranjbar H and Joo S W 2014 *Ind. Eng. Chem. Res.* **53** 1924